Editors' Suggestion | Featured in Physics

Nonlocal Intrinsic Fracture Energy of Polymerlike Networks

Bolei Deng,[1,2,*] Shu Wang,[1,*] Chase Hartquist,[1,*] and Xuanhe Zhao[1,†]
[1]Department of Mechanical Engineering, Massachusetts Institute of Technology, Cambridge, Massachusetts 02139, USA
[2]Computer Science and Artificial Intelligence Laboratory, Massachusetts Institute of Technology, Cambridge, Massachusetts 02139, USA

(Received 9 June 2023; accepted 28 September 2023; published 1 December 2023)

Connecting polymer network fracture to molecular-level chain scission remains a quandary. While the Lake-Thomas model predicts the intrinsic fracture energy of a polymer network is the energy to rupture a layer of chains, it underestimates recent experiments by ~1–2 orders of magnitude. Here we show that the intrinsic fracture energy of polymerlike networks stems from nonlocal energy dissipation by relaxing chains far from the crack tip using experiments and simulations of 2D and 3D networks with varying defects, dispersity, topologies, and length scales. Our findings not only provide physical insights into polymer network fracture but offer design principles for tough architected materials.

DOI: 10.1103/PhysRevLett.131.228102

Polymer networks are the molecular scaffolds that form the basis of materials in a wide range of both common and highly specialized applications, including consumer products (e.g., tires, rubber bands, contact lenses) [1], biomedical implants [2] and soft electronic devices [3]. The lifetime of polymer networks is limited by their fracture, which is characterized by the energy required to propagate a crack per newly created surface area [4]. This energy typically has contributions from bulk dissipation and elastically active structures within the material [5]. The contribution from the latter is known as intrinsic fracture energy [6,7]. As established by Griffith in the 1920s [8], the intrinsic fracture energy of glass can be considered as the energy required to break a layer of atomic bonds, i.e., $\Gamma_0 = MU_{\text{bond}}$, where M is the number of broken atomic bonds per unit created area and U_{bond} is the bond dissociation energy of a single atomic bond [Fig. 1(a)]. Although this simple model semiquantitatively explained the fracture of some hard materials, the intrinsic fracture energy of polymer networks has been found to be several orders of magnitude larger than just that of breaking a single layer of atomic bonds [9].

Lake and Thomas explained this phenomenon in 1967 by connecting the intrinsic fracture energy of polymer networks to the rupture of covalent polymer chains [10]. This model predicts that the intrinsic fracture energy is equal to the number of broken bridging polymer chains per unit created area (M) multiplied by the work to rupture a bridging polymer chain (U_{chain}), i.e., $\Gamma_0 = \Gamma_{\text{LT}} = MU_{\text{chain}}$ [Fig. 1(b)]. During crack propagation, the energy stored in the bridging polymer chains is dissipated after the chains are broken. The Lake-Thomas model has been widely applied to explain experimental data and predict intrinsic fracture energy [11–13]. Recent experiments [14,15], however, indicate that the Lake-Thomas model has also significantly underestimated the intrinsic fracture energy of polymer networks by ~1–2 orders of magnitude (see Table I). Modified models have been proposed to rationalize this underestimate [7,15–17], but these models cannot fully explain the orders of magnitude discrepancy between the Lake-Thomas model and experimental results. This discrepancy implies the potential for nonlocal energy release and dissipation even within well-formed gels that are highly elastic. This is further supported by recent studies on brittle hydrogels [18,19], which suggest the existence of a nonlocal process zone around the crack tip.

In this Letter, we investigate the fracture of generic networks that consist of polymerlike chains across multiple length scales. We find that the intrinsic fracture energy of the network is orders of magnitude greater than the energy required to rupture a single layer of polymer chains. This

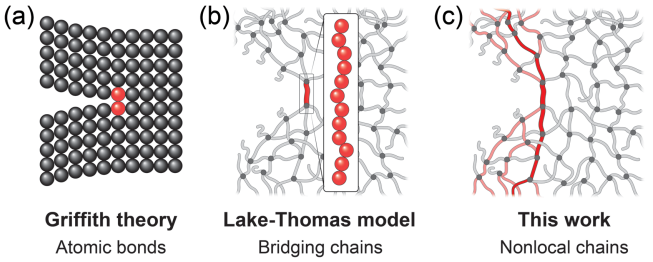

FIG. 1. Intrinsic fracture energy. (a) In Griffith's theory, the intrinsic fracture energy equals the energy needed to break a single layer of atomic bonds. (b) In the Lake-Thomas model, the intrinsic fracture energy equals the energy needed to break a single layer of polymer chains. (c) Our study suggests that the intrinsic fracture energy mainly results from nonlocal energy dissipation by relaxing polymer chains far away from the crack tip and is orders of magnitude higher than Lake-Thomas prediction.

TABLE I. The ratio of experimentally measured intrinsic fracture energy, Γ_0, to the predicted values according to the Lake-Thomas model, Γ_{LT}. These experimental results indicate that the Lake-Thomas model underestimated the intrinsic fracture energy of polymer networks by ~1–2 orders of magnitude.

	Wang *et al.* [20]	Lin *et al.* [7]	Akagi *et al.* [12]	Barney *et al.* [15]
Γ_0/Γ_{LT}	≈77	≈60	≈72	≈150

discrepancy arises because energy is released and dissipated from the relaxation of polymer chains far beyond the crack tip when a bridging chain ruptures [Fig. 1(c)].

We adopt the modified freely jointed chain model (m-FJC) [21] to describe the force-extension dependence of chains. The m-FJC model considers both the conformational entropic elasticity of the polymer chain and the energetic elasticity of backbone bonds (e.g., bond stretching and bending). The relationship between its stretch λ and reaction force f can be written as [21]

$$\frac{\lambda}{\lambda_{\text{lim}}} = \left[\coth\left(\frac{f}{K_S}\right) - \frac{K_S}{f}\right]\left(1 + \frac{f}{K_E}\right), \tag{1}$$

where the parameters K_S and K_E are the soft entropic modulus [Fig. 2(a), blue] and the stiff energetic modulus [Fig. 2(a), red] of the polymer chains, respectively ($K_E \gg K_S$ for typical polymer chains) [22]. The parameter λ_{lim} is the entropic stretch limit beyond which the force increases rapidly due to the deformation of backbone bonds.

To model the fracture of polymerlike networks, we start with 2D samples with triangular lattices consisting of n nodes and e edges [Fig. 2(b)]. Each edge is modeled by a nonlinear spring with initial end-to-end distance r_0 and force-stretch relation $f(\lambda)$ defined in Eq. (1) [29,30]. To further capture the fracture of a polymer chain, the nonlinear spring is set to break at a force f_f with stretch λ_f. In the simulation, clamped boundary conditions are applied to the top and bottom surfaces, which quasistatically stretch the sample from an initial height of h_0 to a height of h. The deformation of the lattices is fully described by the coordinates of every node (x_i, y_i), where $i = 1, \ldots, n$. At each loading step, the total energy of the system is obtained by summing the elastic energy of every spring:

$$U_{\text{total}} = \sum_{i,j} \int_1^{\lambda_{ij}} f(\lambda')d\lambda', \tag{2}$$

where $\lambda_{ij} = r_0^{-1}\sqrt{(x_i - x_j)^2 + (y_i - y_j)^2}$ is the stretch of the edge connecting node i with j. The coordinates of each node (x_i, y_i) are then numerically determined by minimizing U_{total} using Newton's method in MATLAB. Additionally, if $\lambda_{ij} > \lambda_f$, which indicates that the edge connecting nodes i and j has broken, this edge will be removed from the lattice for future steps (see numerical details in the Supplemental Material [31], Sec. S2). To measure the intrinsic fracture energy of a given network, we perform the pure shear test [4]. This includes two steps: (i) load a notched sample to the point where the bridging chain breaks and record the critical height of the sample h_c; (ii) load an unnotched sample and record the nominal stress as a function of sample height h [Fig. 2(b)]. The intrinsic fracture energy of the network is then calculated as

$$\Gamma_0 = \int_{h_0}^{h_c} s dh, \tag{3}$$

where s is the nominal stress of the unnotched sample. The value of Γ_0 is an intrinsic property of the network and is size independent, provided the network is sufficiently large. For polymerlike networks with $K_E \gg K_S$, a converged

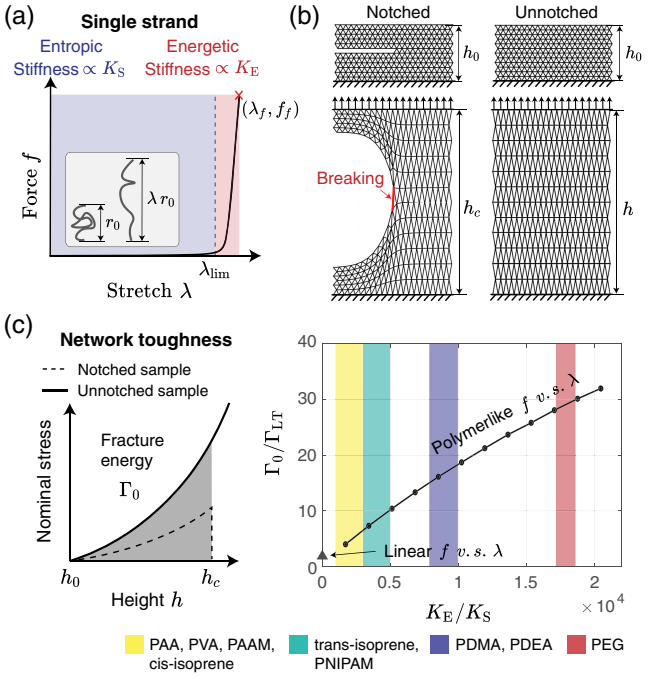

FIG. 2. Intrinsic fracture energy of polymerlike networks. (a) A single strand is governed by a strongly nonlinear force-stretch curve, with a long, soft entropic part characterized by a modulus K_S and a short, stiff energetic part characterized by a modulus K_E. (b) To measure the intrinsic fracture energy of polymerlike networks, a pure shear test is conducted. (c) The intrinsic fracture energy Γ_0 of polymerlike networks with different ratios of K_E/K_S (solid line) compared to a network consisting of linear chains (triangular marker). These results are obtained from numerical simulations under quasistatic loading conditions. Parameters K_S and K_E are taken from the single-molecule force spectroscopy experiments of different polymers: poly (acrylic acid) (PAA) [23], poly (vinyl alcohol) (PVA) [24], polyisoprene [25], poly(acryl amide) (PAAM) and poly(N-isopropyl acrylamide) (PNIPAM) [26], poly(dimethylacrylamide) (PDMA) and poly(diethylacrylamide) (PDEA) [27], and poly(ethylene glycol) (PEG) [28].

value of Γ_0 requires a significantly large sample, typically containing over 1000 layers of chains (see Supplemental Material [31], Sec. S2.4 for convergence studies).

Using a sufficiently large sample with 4000 layers, we calculate the fracture energies Γ_0 of the polymerlike networks with a wide range of K_E/K_S values and compare them to the Lake-Thomas predictions, i.e., $\Gamma_{LT} = MU_{chain}$. Parameters K_E and K_S are taken from reported single-molecule force spectroscopy (SMFS) experimental results of different polymers that use the m-FJC model as the fitting function. As shown in Fig. 2(c), Γ_0/Γ_{LT} is significantly larger than unity for all networks with polymerlike chains. This phenomenon is closely linked to the nonlinearity of the force-stretch behavior of the polymerlike chains, as Γ_0/Γ_{LT} increases with K_E/K_S. Notably, when we use linear springs to model the chains, the ratio Γ_0/Γ_{LT} nears the expectation of the Lake-Thomas model (triangular marker). These results emphasize that the force-extension relationship of chains directly affects the intrinsic fracture energy of polymerlike networks.

To assess the generality of our findings, we conduct additional simulations that investigate the impact of inhomogeneities, defects, and lattice topologies on the intrinsic fracture energy of polymerlike networks. Specifically, we feature the PEG-like chain with $K_E/K_S = 1.8 \times 10^4$ and examine the intrinsic fracture energy of irregular networks [lattices with dispersed edge lengths, Fig. 3(a)] and networks with dangling chains [lattices with missing edges, Fig. 3(b)]. Unsurprisingly, we find that these defected networks retain large Γ_0/Γ_{LT} ratios. Different topologies, including triangular, square, and hexagonal lattices, along with 3D diamond cubic lattices are also investigated with various K_E/K_S ratios. Figure 3(c) shows that increasing chain nonlinearity leads to a magnifying trend of Γ_0/Γ_{LT} in different 2D lattice topologies, where the hexagonal lattice exhibits relatively higher fracture energy due to its larger loop size [17,38–40]. A similar trend is also observed in the 3D diamond cubic network [Fig. 3(d)]. These results signify that more chain nonlinearity leading to a higher Γ_0/Γ_{LT} is a universal phenomenon, regardless of lattice topology or dimensionality. These numerical results are consistent with recent experimental findings [7,12,15,20] showing that the intrinsic fracture energy of polymer networks can be significantly larger than the values predicted by the Lake-Thomas model (see Table S1, Supplemental Material [31]).

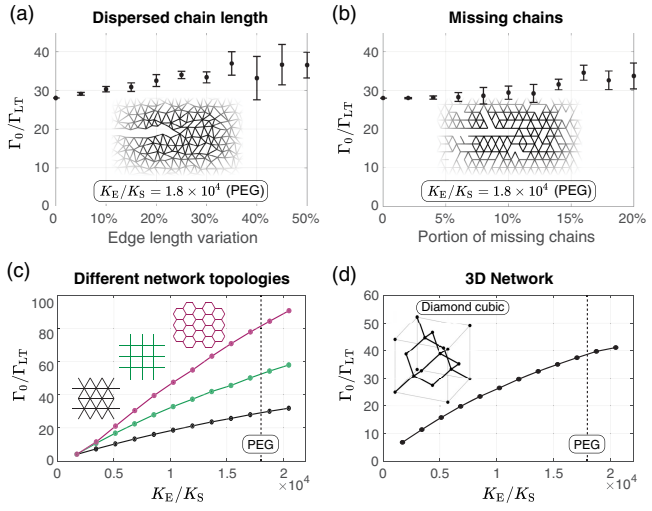

FIG. 3. Generality of elevated intrinsic fracture energy in polymerlike networks. (a) Intrinsic fracture energy of irregular networks with dispersed edge lengths, with variations ranging from 0% to 50%, and (b) networks with missing chains ranging from 0% to 20%. Both (a) and (b) are based on single strands with $K_E/K_S = 1.8 \times 10^4$ (PEG chains). Intrinsic fracture energy of networks with (c) different 2D topologies, including triangular, square, and hexagonal lattices, and (d) 3D diamond cubic lattices for varying K_E/K_S ratios.

To further understand the anomalously high intrinsic fracture energy of polymerlike networks, we investigate the behavior of chains near the crack tip [Fig. 4(a)] by comparing networks of PEG-like chains to those with linear elastic chains. The strain energy distributions of the two networks just prior to the fracture of a chain are shown in Fig. 4(b), where the color indicates the energy on each chain normalized by the work to rupture a single chain U_{chain}. Notably, the energy distribution of the PEG network is clearly nonlocal when contrasted to the network with linear chains, where the energy is concentrated in the one or two layers nearest to the crack tip. We therefore postulate that for polymerlike networks, the abnormally high ratio of Γ_0/Γ_{LT} is predominantly due to nonlocal energy dissipation by the relaxation of chains distant from the crack tip. To test this hypothesis, we analyze the released energy of each chain, which is defined by the energy difference before and after the fracture of a single chain at the crack tip. The Lake-Thomas model predicts the released energy of the broken chain contributes to the overall intrinsic fracture energy of the network. This is qualitatively true for the network consisting of chains with linear elasticity, where the major energy release is limited to a relatively confined zone around the crack tip [e.g., ~1–2 layers Fig. 4(c), top]. However, for the network of PEG-like chains, even chains far away from the crack tip (e.g., > 20 layers) release a significant amount of energy after the rupture of a single chain at the crack tip. The released energy is then converted into kinetic energy in the network and is eventually dissipated.

To investigate where and how the released energy is dissipated, we establish a spring-mass model to simulate the dynamic process upon the fracture of a chain at the crack tip until a new equilibrium is reached. When a bridging chain ruptures, the tension on the bridging chain suddenly vanishes, and other junctions in the network continuum are not balanced. The elastic energy stored in the continuum is then released and becomes the kinetic

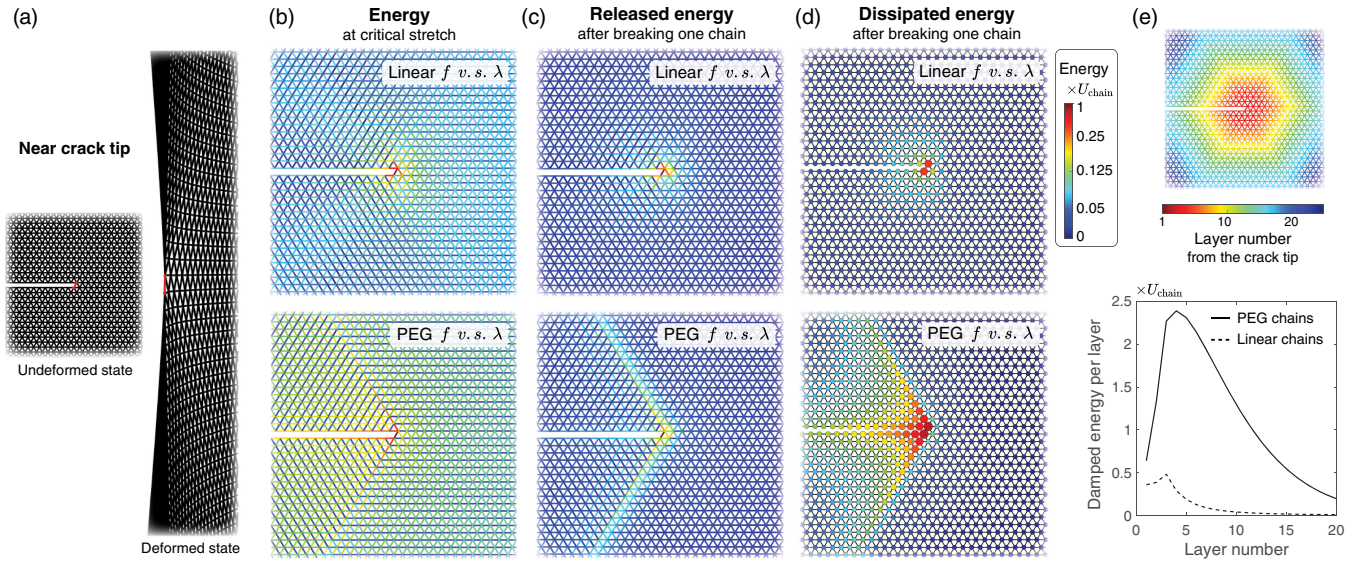

FIG. 4. Nonlocal energy release and dissipation during fracture of polymerlike networks: (a) Visualization of the polymerlike network near the crack tip in the undeformed and deformed states. (b) Energy stored in each chain just before a chain breaks at the crack tip. (c) Energy released by each chain after a chain breaks. (d) Energy dissipated at each node after a chain breaks. In (b)–(d), the top row presents results for networks with linear chains, while the bottom row presents networks with PEG chains. The energy on each chain is normalized by the work to rupture a single chain U_{chain}. (e) Damped energy as a function of the layer number away from the crack tip for networks consisting of PEG chains (solid line) and linear chains (dashed line).

energy of the junctions. In real polymer networks, the energy released from the network continuum is damped by the relaxation of both broken and unbroken polymer chains, and eventually dissipated as heat. To damp the kinetic energy induced by the chain breaking in our simulated network, we implement viscous damping on every node of the lattice. Unlike dynamic fracture [41–43], we aim to investigate the intrinsic fracture energy of polymerlike networks, under conditions by which the crack velocity approaches zero. Therefore, the network was deformed quasistatically as previously mentioned and set to be overdamped to mitigate potential dynamic effect. The total damped energy throughout this process is recorded and shown in Fig. 4(d). To provide a more quantitative comparison, we present the total damped energy as a function of layer number from the crack tip in Fig. 4(e). In stark contrast to linear networks (dashed line) where most of the energy is damped near the crack tip, the polymerlike network (solid line) dissipates much more energy through chains far away from the crack tip; this eventually leads to the high ratio of $\Gamma_0/\Gamma_{\text{LT}}$. With the same U_{chain}, a network made from polymerlike chains is much tougher than that made from chains with linear elasticity. Additionally, the ratio $\Gamma_0/\Gamma_{\text{LT}}$ provides insight into the spatial extent of the dissipation zone, quantified in terms of the layers of chains (see Supplemental Material [31], Sec. 2.3.2 for details).

Finally, in order to experimentally validate our findings, we fabricated macroscopic architected materials that consist of polymerlike strands. Specifically, each strand was produced by laser cutting (model: Epilog Zing 24 60 W) an Acetal Film (semi-clear white, 0.003" thick, McMaster-Carr) into an initially folded ribbon. The ribbon-shaped strand is designed to mimic the force-extension behavior of polymer chains, with a soft initial unfolding followed by a stiff stretching upon loading [44]. The former corresponds to the "entropic stiffness," while the latter corresponds to the "energetic stiffness." This results in a ratio of energetic to entropic stiffness $K_{\text{E}}/K_{\text{S}} \approx 800$ [Fig. 5(a)]. To test the intrinsic fracture energy of this architected material, ribbon strands are connected into a triangular lattice [Fig. 5(b)]. Tensile tests are performed to obtain the force-stretch curve for the unnotched sample [Fig. 5(c), black solid curve] and the critical height h_c for the notched sample (red solid line, see Supplemental Material [31], Sec. 3 for fabrication and testing details). The measured intrinsic fracture energy of the network is significantly higher than that predicted by the Lake-Thomas model, with $\Gamma_0/\Gamma_{\text{LT}} = 5.57$. Furthermore, simulations of the network using the experimentally determined force-stretch curves for each strand match the experimental results for both notched and unnotched samples, yielding a similar $\Gamma_0/\Gamma_{\text{LT}} = 5.61$ with an error of only 0.7%. These experiments not only validate the accuracy of our simulations but also demonstrate a new approach to designing ultratough architected materials by engineering the force-stretch response of individual strands.

In this Letter, we have demonstrated that the Lake-Thomas model underestimates the intrinsic fracture energy of polymerlike networks by more than an order of magnitude, even if the networks are purely elastic with latticelike topology [45–47]. Our experimental and numerical analyses reveal that this discrepancy arises from significant

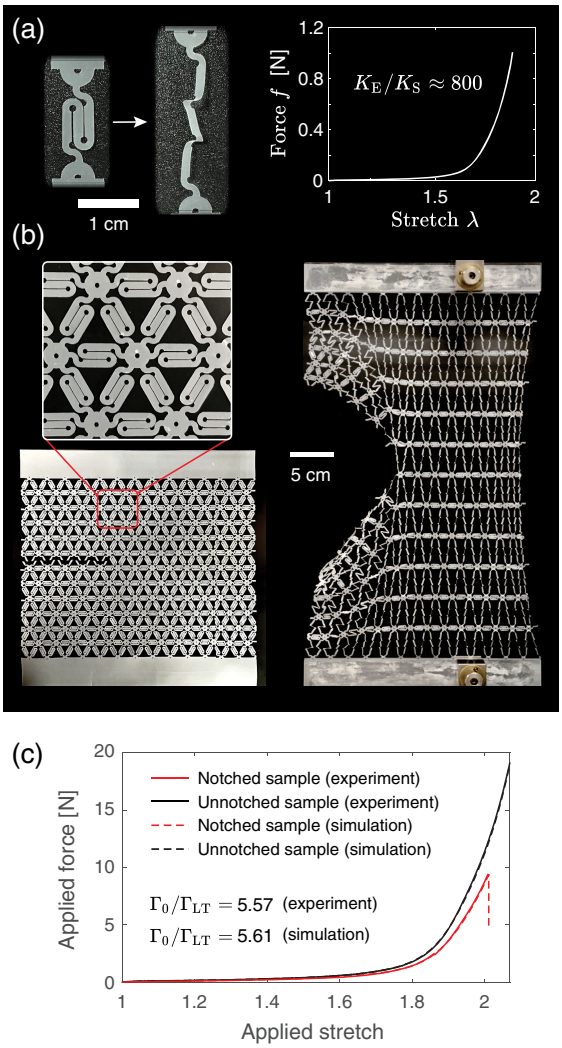

FIG. 5. Experimental validation of the polymerlike behavior and enhanced intrinsic fracture energy in architected materials. (a) Force-stretch response of an architected strand fabricated to mimic the behavior of polymer chains, with a ratio of energetic to entropic stiffness $K_E/K_S \approx 800$. (b) A laser cut architected material consists of polymerlike strands. The pure shear test is performed to measure its intrinsic fracture energy. (c) Pure shear tests on the architected materials via experiments (solid lines) and simulations (dashed lines).

energy release and dissipation far from the crack tip, rather than solely in the bridging chain. We show that this nonlocal intrinsic fracture energy is strongly connected to the high nonlinearity of the force-extension relation and the abrupt breaking of polymer chains. Our findings provide implications for the mechanics of real polymer networks and designing metamaterials. For real polymer networks, our results indicate that the released or dissipated energy per broken chain is inherently larger than the work to rupture a single chain. For metamaterials, our results indicate that high toughness and resilience can be obtained by controlling the nonlinear mechanics of the constituent architected chains. Future directions could involve exploring the relationship between the network structure and the intrinsic fracture energy, as well as investigating the effect of defects and inhomogeneities in the network on its mechanical properties. Moreover, our findings could be extended to other materials, such as ultratough structures, soft matter and biomaterials, with implications for a wide range of applications, including aircraft, space vehicles, and tissue engineering.

We thank Bohan Wang for his guidance during the implementation of our simulations. This work is supported in part by the National Institutes of Health (Grants No. 1R01HL153857-01 and No. 1R01HL167947-01), the National Science Foundation (Grant No. EFMA-1935291), and Department of Defense Congressionally Directed Medical Research Programs (Grant No. PR200524P1).

*These authors contributed equally to this work.
†zhaox@mit.edu

[1] W. V. Mars and A. Fatemi, A literature survey on fatigue analysis approaches for rubber, Int. J. Fatigue **24**, 949 (2002).
[2] Tineke De Coninck, Wouter Huysse, Laurent Willemot, René Verdonk, Koenraad Verstraete, and Peter Verdonk, Two-year follow-up study on clinical and radiological outcomes of polyurethane meniscal scaffolds, Am. J. Sports Med. **41**, 64 (2013).
[3] Samuel E. Root, Suchol Savagatrup, Adam D. Printz, Daniel Rodriquez, and Darren J. Lipomi, Mechanical properties of organic semiconductors for stretchable, highly flexible, and mechanically robust electronics, Chem. Rev. **117**, 6467 (2017).
[4] R. S. Rivlin and A. Gr Thomas, Rupture of rubber. I. Characteristic energy for tearing, J. Polym. Sci. **10**, 291 (1953).
[5] Xuanhe Zhao, Multi-scale multi-mechanism design of tough hydrogels: Building dissipation into stretchy networks, Soft Matter **10**, 672 (2014).
[6] Ruobing Bai, Jiawei Yang, and Zhigang Suo, Fatigue of hydrogels, Eur. J. Mech.-A/Solids **74**, 337 (2019).
[7] Shaoting Lin and Xuanhe Zhao, Fracture of polymer networks with diverse topological defects, Phys. Rev. E **102**, 052503 (2020).
[8] Alan Arnold Griffith, VI. The phenomena of rupture and flow in solids, Phil. Trans. R. Soc. A **221**, 163 (1921).
[9] G. J. Lake and P. B. Lindley, The mechanical fatigue limit for rubber, J. Appl. Polym. Sci. **9**, 1233 (1965).
[10] G. J. Lake and A. G. Thomas, The strength of highly elastic materials, Proc. Phys. Soc. London Sect. A **300**, 108 (1967).
[11] Jun Cui, Melissa A. Lackey, Gregory N. Tew, and Alfred J. Crosby, Mechanical properties of end-linked PEG/PDMS hydrogels, Macromolecules **45**, 6104 (2012).
[12] Yuki Akagi, Jian Ping Gong, Ung-il Chung, and Takamasa Sakai, Transition between phantom and affine network model observed in polymer gels with controlled network structure, Macromolecules **46**, 1035 (2013).

[13] Junsoo Kim, Guogao Zhang, Meixuanzi Shi, and Zhigang Suo, Fracture, fatigue, and friction of polymers in which entanglements greatly outnumber cross-links, Science **374**, 212 (2021).
[14] Yuki Akagi, Hayato Sakurai, Jian Ping Gong, Ung-il Chung, and Takamasa Sakai, Fracture energy of polymer gels with controlled network structures, J. Chem. Phys. **139**, 144905 (2013).
[15] Christopher W. Barney, Ziyu Ye, Ipek Sacligil, Kelly R. McLeod, Han Zhang, Gregory N. Tew, Robert A. Riggleman, and Alfred J. Crosby, Fracture of model end-linked networks, Proc. Natl. Acad. Sci. U.S.A. **119**, e2112389119 (2022).
[16] Shu Wang, Sergey Panyukov, Michael Rubinstein, and Stephen L. Craig, Quantitative adjustment to the molecular energy parameter in the Lake–Thomas theory of polymer fracture energy, Macromolecules **52**, 2772 (2019).
[17] Shu Wang, Sergey Panyukov, Stephen L. Craig, and Michael Rubinstein, Contribution of unbroken strands to the fracture of polymer networks, Macromolecules **56**, 2309 (2023).
[18] Chenzhuo Li, Xinyue Wei, Meng Wang, Mokhtar Adda-Bedia, and John M. Kolinski, Crack tip kinematics reveal the process zone structure in brittle hydrogel fracture, J. Mech. Phys. Solids **178**, 105330 (2023).
[19] Yudong Pan, Yifan Zhou, Zhigang Suo, and Tongqing Lu, Inelastic zone around crack tip in polyacrylamide hydrogel identified using digital image correlation, Eng. Fract. Mech. **289**, 109435 (2023).
[20] Shu Wang, Haley K. Beech, Brandon H. Bowser, Tatiana B. Kouznetsova, Bradley D. Olsen, Michael Rubinstein, and Stephen L. Craig, Mechanism dictates mechanics: A molecular substituent effect in the macroscopic fracture of a covalent polymer network, J. Am. Chem. Soc. **143**, 3714 (2021).
[21] Steven B. Smith, Yujia Cui, and Carlos Bustamante, Overstretching b-DNA: The elastic response of individual double-stranded and single-stranded DNA molecules, Science **271**, 795 (1996).
[22] Wenke Zhang and Xi Zhang, Single molecule mechanochemistry of macromolecules, Prog. Polym. Sci. **28**, 1271 (2003).
[23] Hongbin Li, Bingbing Liu, Xi Zhang, Chunxiao Gao, Jiacong Shen, and Guangtian Zou, Single-molecule force spectroscopy on poly (acrylic acid) by AFM, Langmuir **15**, 2120 (1999).
[24] Hongbin Li, Wenke Zhang, Xi Zhang, Jiacong Shen, Bingbing Liu, Chunxiao Gao, and Guangtian Zou, Single molecule force spectroscopy on poly (vinyl alcohol) by atomic force microscopy, Macromol. Rapid Commun. **19**, 609 (1998).
[25] WK Zhang, Nano-mechanical detection of single molecules, Ph.D. thesis, Jilin University, 2002.
[26] Wenke Zhang, Shan Zou, Chi Wang, and Xi Zhang, Single polymer chain elongation of poly (n-isopropylacrylamide) and poly (acrylamide) by atomic force microscopy, J. Phys. Chem. B **104**, 10258 (2000).
[27] Chi Wang, Weiqing Shi, Wenke Zhang, Xi Zhang, Yukiteru Katsumoto, and Yukihiro Ozaki, Force spectroscopy study on poly (acrylamide) derivatives: Effects of substitutes and buffers on single-chain elasticity, Nano Lett. **2**, 1169 (2002).
[28] F. Oesterhelt, M. Rief, and H. E. Gaub, Single molecule force spectroscopy by AFM indicates helical structure of poly (ethylene-glycol) in water, New J. Phys. **1**, 6 (1999).
[29] Yunwei Mao, Brandon Talamini, and Lallit Anand, Rupture of polymers by chain scission, Extreme Mech. Lett. **13**, 17 (2017).
[30] Brandon Talamini, Yunwei Mao, and Lallit Anand, Progressive damage and rupture in polymers, J. Mech. Phys. Solids **111**, 434 (2018).
[31] See Supplemental Material at http://link.aps.org/supplemental/10.1103/PhysRevLett.131.228102 for additional details on calculations, experiments, and simulations, which includes Refs. [32–37].
[32] Hubert M. James and Eugene Guth, Theory of the elastic properties of rubber, J. Chem. Phys. **11**, 455 (1943).
[33] Michael Rubinstein, Ralph H. Colby *et al.*, *Polymer Physics* (Oxford University Press, New York, 2003), Vol. 23.
[34] Bobin Lee, Zhenbin Niu, Junpeng Wang, Carla Slebodnick, and Stephen L. Craig, Relative mechanical strengths of weak bonds in sonochemical polymer mechanochemistry, J. Am. Chem. Soc. **137**, 10826 (2015).
[35] Shaoting Lin, Jiahua Ni, Dongchang Zheng, and Xuanhe Zhao, Fracture and fatigue of ideal polymer networks, Extreme Mech. Lett. **48**, 101399 (2021).
[36] Hanako Asai, Kenta Fujii, Takeshi Ueki, Takamasa Sakai, Ung-il Chung, Masayoshi Watanabe, Young-Soo Han, Tae-Hwan Kim, and Mitsuhiro Shibayama, Structural analysis of high performance ion-gel comprising tetra-PEG network, Macromolecules **45**, 3902 (2012).
[37] Chao Chen, Zhengjin Wang, and Zhigang Suo, Flaw sensitivity of highly stretchable materials, Extreme Mech. Lett. **10**, 50 (2017).
[38] W. Michalke, M. Lang, S. Kreitmeier, and D. Göritz, Comparison of topological properties between end-linked and statistically cross-linked polymer networks, J. Chem. Phys. **117**, 6300 (2002).
[39] Michael Lang, Stefan Kreitmeier, and Dietmar Göritz, Trapped entanglements in polymer networks, Rubber Chem. Technol. **80**, 873 (2007).
[40] Sergey Panyukov, Loops in polymer networks, Macromolecules **52**, 4145 (2019).
[41] Lambert Ben Freund, *Dynamic Fracture Mechanics* (Cambridge University Press, Cambridge, England, 1998).
[42] Markus J. Buehler, Farid F. Abraham, and Huajian Gao, Hyperelasticity governs dynamic fracture at a critical length scale, Nature (London) **426**, 141 (2003).
[43] Jens A. Hauch, Dominic Holland, M. P. Marder, and Harry L. Swinney, Dynamic fracture in single crystal silicon, Phys. Rev. Lett. **82**, 3823 (1999).
[44] Kyung-In Jang, Ha Uk Chung, Sheng Xu, Chi Hwan Lee, Haiwen Luan, Jaewoong Jeong, Huanyu Cheng, Gwang-Tae Kim, Sang Youn Han, Jung Woo Lee *et al.*, Soft network composite materials with deterministic and bio-inspired designs, Nat. Commun. **6**, 6566 (2015).
[45] R. Thomson, C. Hsieh, and V. Rana, Lattice trapping of fracture cracks, J. Appl. Phys. **42**, 3154 (1971).
[46] W. A. Curtin, On lattice trapping of cracks, J. Mater. Res. **5**, 1549 (1990).
[47] M. Marder, Effects of atoms on brittle fracture, Int. J. Fracture **130**, 517 (2004).

Supporting Information for *Nonlocal intrinsic fracture energy of polymer-like networks*

September 25, 2023

S1 Summary of Previous Experimental Data of End-linked Poly(ethylene glycol) (PEG) Gels

The fracture energy of polymer networks has been studied across polymeric systems and compared with the Lake-Thomas model. Since end-linked poly(ethylene glycol) gels are known to have relatively small amount of defects and trapped entanglements, we herein summarize some experimental data from these gels and compare them to the values predicted by the Lake-Thomas model. The shear moduli and fracture energies of these PEG gels are summarized in Table S1.

To make predictions based on the Lake-Thomas model $\Gamma_{\text{LT}} = MU_{\text{chain}}$, we estimate the single-chain energy U_{chain} using the single-molecule force spectroscopy (SMFS) data from Oesterhelt et al. (*1*) The modified freely jointed chain model (m-FJC) describes the relationship between the force *f* and the end-to-end distance *R* of the polymer chain,

$$\frac{R}{L_0} = \left[\coth(\frac{f}{K_{\text{S}}}) - \frac{K_{\text{S}}}{f}\right](1 + \frac{f}{K_{\text{E}}}), \tag{S1}$$

where L_0 is the unperturbed contour length of the polymer. The entropic K_{S} and energetic K_{E} parameters determine the soft entropic elasticity at the low force regime and the stiff energetic

elasticity at high force regime, respectively. For PEG polymers, K_{S} = 5.86 pN and K_{E} = 105 nN (*1*).

To estimate the average L_0 of the elastically active chains of the PEG gels summarized in Table S1, we use the phantom model (*2*) of network elasticity (functionality = 4) for the shear modulus *G* and assume the reaction extent of cross-linking is 100%,

$$G = (\nu - \mu)kT = \frac{1}{2}\nu kT = \frac{1}{2}\frac{cRT}{M_x}, \tag{S2}$$

where ν is the number density of elastically active chains, μ is the number density of elastically active junctions ($\mu = \nu/2$ when functionality is four), k is Boltzmann constant, T is absolute temperature, c is the mass concentration the polymer, and M_x is the average molecular weight of elastically active chains. Given the molar mass of PEG Kuhn segment M_0 is 137 g/mol and the Kuhn length b is 1.1 nm, (*3*) the average contour length of elastically active chains within each PEG network can be calculated (L_0 = M_x/137 g/mol $\times$ 1.1 nm). Combining L_0 for different gels with the single-chain breaking force f_f and parameters K_{S} and K_{E} from before, the single-chain energy U_{chain} is calculated for each gel using Eq. (S3) below (*4*). Eq. (S4) is obtained by integrating the inverse function of Eq. (S1).

$$U_{\text{chain}} = L_0 K_{\mathrm{S}} \left\{ (\frac{f_f}{K_{\mathrm{S}}}) \left[\coth(\frac{f_f}{K_{\mathrm{S}}}) - \frac{K_{\mathrm{S}}}{f_f} \right] + \ln(\frac{f_f/K_{\mathrm{S}}}{\sinh f_f/K_{\mathrm{S}}}) + \frac{f_f^2}{2K_{\mathrm{S}}K_{\mathrm{E}}} \right\}. \tag{S3}$$

For $f_f \gg K_{\mathrm{S}}$ (synthetic covalent polymers usually have $f_f/K_{\mathrm{S}} \approx 1000$), an asymptotic form can be used,

$$U_{\text{chain}} \simeq L_0 K_{\mathrm{S}} \left\{ (\frac{f_f}{K_{\mathrm{S}}}) \left[\coth(\frac{f_f}{K_{\mathrm{S}}}) - \frac{K_{\mathrm{S}}}{f_f} \right] + \left[\ln(\frac{f_f}{K_{\mathrm{S}}}) - \frac{f_f}{K_{\mathrm{S}}} - \ln 0.5 \right] + \frac{f_f^2}{2K_{\mathrm{S}}K_{\mathrm{E}}} \right\}. \tag{S4}$$

The single-chain breaking force f_f for elastically active PEG chains are summarized in Table S1. Note that the forces f_f of gels by Wang et al. (*5*) and Barney et al. (*6*) are considered to be substantially smaller than typical breaking force of C-C or C-O bonds ($\approx$ 5 nN). This is because the backbone of the elastically active chains contain weaker bonds. The gels made by

Wang et al. (*5*) contain a triazole group on the chain backbone that make them prone to break at the alpha C-C bond of the triazole group ($\approx$ 3.8 nN), while the gels made by Barney et al. (*6*) contain a C-S backbone bond that breaks at $\approx$ 2.5 nN (*7*). The forces f_f of gels by Lin et al. (*8*) and Akagi et al. (*9*) are considered to be close to 5 nN since all the chemical bonds on the backbone are similarly strong as common C-C and C-O bonds. The values for U_{chain} for elastically active chains in each gel are summarized in Table S1.

The areal number density M of elastically active chains for each gel can be estimated by $M \approx \frac{1}{2}\nu R_0$ (*10*), where $R_0 \approx bN^{0.588}$ is the undeformed end-to-end distance of the elastically active chains. The real chain scaling is applied based on the assumption that chains are at or slightly above overlap under the preparation condition and that the solvent is a good solvent, like water (*11*) (note that Wang et al. (*5*) and Barney et al. (*6*) prepared their gels in propylene carbonate and dimethyl sulfoxide, respectively). Therefore, the fracture energy predicted by the Lake-Thomas model can be calculated using $\Gamma_{\text{LT}} = MU_{\text{chain}}$. The estimated values of Γ_{LT} are summarized in Table S1. When compared to the experimental intrinsic fracture energy Γ_0, the ratios $\Gamma_0/\Gamma_{\text{LT}}$ are all much larger than unity. This discrepancy motivated us to investigate the relationship between single-chain energy and the tearing energy of the network.

We acknowledge that the energy U_{chain} was historically estimated by number of chemical bonds times the bond dissociation energy of the chemical bonds ($U_{\text{chain}} = N \times U_{\text{BDE}}$) (*6, 12*). However, a recent modification considering the mechanochemical reactivity of chemical bonds suggests that U_{chain} could be better estimated by the total area under the force-displacement curve of a polymer chain to its breaking point. We therefore estimate U_{chain} with this modified method throughout the paper, which has been discussed in detail by Wang et al. (*4, 5*).

In the main text, we use a numerical simulation to show that the energy release from networks is non-local even for defect-free networks. Node dynamics damp the released energy in dynamic simulations. We set the network to be overdamped while investigating the critical

tearing energy of the network to mitigate dynamic influences on crack propagation and reduce the crack velocity towards zero. In real polymer networks, however, damping effects are more complicated. To investigate damping effects, let us consider a simplified case where a chain in a dilute solution is displaced from one end while the other is kept fixed. If the pulled chain end is released in the bond stretching regime where the end-to-end distance is larger than the force-free contour length, the critical damping coefficient of the monomer at the displaced end can be calculated using $c_c = 2\sqrt{K_{\text{seg}} m_{\text{mon}}}$. The segment elasticity K_{seg} of a PEG Kuhn monomer is 150 N/m (*1*), while the mass m_{mon} is 2.27 $\times$ 10^{-22} g (*3*). The calculated critical damping coefficient is 3.7 $\times$ 10^{-10} Ns/m when the end-to-end distance is larger than the force-free contour length. However, once the end-to-end distance becomes much smaller than the contour length of the chain, entropic elasticity dominates. The critical damping coefficient of the monomer at the displaced end in the entropic linear elastic regime can be estimated using $c_c = 2\sqrt{3K_{\text{seg}} m_{\text{mon}}/L_0}$, where L_0 is the force-free contour length. For a typical chain with a contour length of 100 nm, the critical damping parameter for a Kuhn monomer in the regime with entropic elasticity can be estimated to be around 4 $\times$ 10^{-13} Ns/m.

On the other hand, the damping coefficient for a Kuhn monomer can be calculated based on Stokes law $c \approx 6\pi\eta_s b$, where η_s is the solvent viscosity and b is the Kuhn length. Parameters for PEG ($b \approx 1.1$ nm) (*3*) in water ($\eta_s \approx 10^{-3}$ Pa/s) yield a damping coefficient around 10^{-11} Ns/m. Hence, the damping ratio $\beta = c/c_c$ for the monomer at the displaced end is on the order of 10^{-1} when the end-to-end distance is larger than its contour length, and it is on order of 10^2 when the chain enters the entropic linear elastic regime. We acknowledge that the damping of polymer chains at high strain and high force is a complicated process. This simple calculation aims to show that polymer networks are likely to be underdamped at high strain and highly overdamped at low strain.

	Wang et al. (*5*)	Lin et al. (*13*)	Akagi et al. (*9*)	Barney et al. (*6*)
G [kPa]	24.4	10.6	37	17.4
Γ_0 [J/m^2]	27.1	34	22	25.1
f_f [nN]	3.8	5.0	5.0	2.5
U_{chain} [nN· nm] [a]	5.5	14.7	4.6	3.6
M [m^{-2}] [b]	6.3×10^{16}	3.9×10^{16}	6.8×10^{16}	4.8×10^{16}
Γ_{LT} [J/m^2] [c]	0.35	0.57	0.31	0.17
$\Gamma_{\mathbf{0}}/\Gamma_{\mathbf{LT}}$	$\approx$ **77**	$\approx$ **60**	$\approx$ **72**	$\approx$ **150**

Table S1: Experimental results of measured shear modulus *G* and intrinsic fracture energy Γ_0 for PEG gels and their corresponding estimates based on the Lake-Thomas model $\Gamma_{\text{LT}} = MU_{\text{chaiSn}}$. [a]Single-chain energy U_{chain} is estimated using single-molecule force spectroscopy (SMFS) data by Oesterhelt et al. (*1*) and the storage moduli.[b]Areal number densities M are estimated based on the moduli reported. [c]Note that about 90% of the gels is solvent.

S2 Numerical Simulation

This section outlines the implementation details of the simulator used to evaluate the intrinsic fracture energy of the networks.

S2.1 Mathematical model

The polymer-like network is modeled by a system of connected nonlinear springs with stretch λ and reaction force f relations characterized by the modified freely jointed chain model Eq. (S6). If the initial length of the polymer chain is defined as R_0, then the end-to-end distance R and unperturbed contour length L_0 can be expressed as a function of stretch as,

$$R = \lambda R_0, \text{ and } L_0 = \lambda_0 R_0, \tag{S5}$$

where λ_0 is the crossover stretch when the polymer-like chain reaches its contour length and transitions between entropic and energetic elasticity. The left-hand side of Eq. (S6) can therefore be attained by dividing R/L_0 to give λ/λ_0. The model then yields a relation between force f and stretch λ as,

$$\frac{\lambda}{\lambda_0} = \left[\coth(\frac{f}{K_{\text{S}}}) - \frac{K_{\text{S}}}{f}\right](1 + \frac{f}{K_{\text{E}}}), \tag{S6}$$

which yields the constitutive law of each nonlinear spring used in the simulation. To further capture the fracture of a polymer chain, the nonlinear spring is set to break at a force f_f with stretch λ_f. For PEG chains, prior experimental results indicate that K_S = 5.86 pN and K_E = 105 nN (*1*). We further set a breaking force of $f_f = 5$ nN and $\lambda_0 = 5$ to ensure a large polymer-like stretch. PEG chains result in a $K_\mathrm{E}/K_\mathrm{S}$ ratio of $\sim 1.8 \times 10^4$, which quantitatively shows the stiffness difference between the energetic and entropic constitutive regimes. In Fig. S1, we present stretch-force curves of polymer chains with different ratios of $K_\mathrm{E}/K_\mathrm{S}$. As shown in Fig. S1, a larger ratio of $K_\mathrm{E}/K_\mathrm{S}$ results in a stretch-force curve with accentuated nonlinearity.

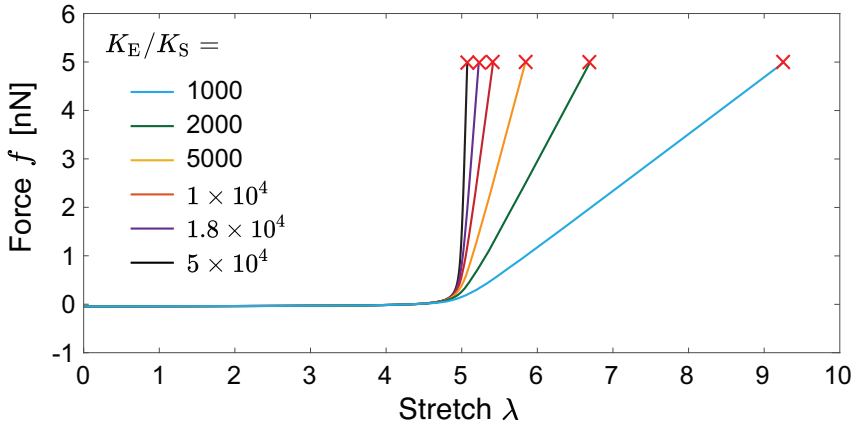

Figure S1: Force-stretch curves described by Eq. (S6) with different ratios of $K_\mathrm{E}/K_\mathrm{S}$. In all these cases, the chain is set to break at $\lambda_f = 5$ and $f_f = 5$ nN.

To simulate general 3D lattices consisting of n nodes and e edges, we describe the lattice deformation through the coordinates of every node (x_i, y_i, z_i), where $i = 1, ..., n$. The node coordinates and their connectivity are saved in two matrices in MATLAB. At each loading step, the total energy in the system can be expressed by summing the elastic energy of each edge or spring as,

$$U_\mathrm{total} = \sum_{i,j} \int_1^{\lambda_{ij}} f(\lambda')d\lambda', \tag{S7}$$

where λ_{ij} is the stretch of the edge connecting node i with j:

$$\lambda_{ij} = r_0^{-1}\sqrt{(x_i - x_j)^2 + (y_i - y_j)^2 + (z_i - z_j)^2}, \tag{S8}$$

The coordinates of each node (x_i, y_i, z_i) are then numerically obtained by minimizing U_{total} through solving

$$\frac{\partial U_{\text{total}}}{\partial x_i} = 0, \ \frac{\partial U_{\text{total}}}{\partial y_i} = 0, \ \frac{\partial U_{\text{total}}}{\partial z_i} = 0, \tag{S9}$$

using Newton's method in MATLAB. Additionally, if $\lambda_{ij} > \lambda_f$, which indicates that the edge connecting nodes i and j has broken, the edge is removed from the lattice by permanently deleting the corresponding rows and columns in the connectivity matrices.

In the simulation, clamped boundary conditions are applied to the top and bottom surfaces, which quasi-statically stretch the sample from an initial height of h_0 to a height of h in the z-direction. This is realized by applying displacement boundary conditions on the top and bottom nodes as,

$$\begin{aligned} z_i &= h, \text{ for } i \in \text{top nodes}, \\ z_i &= z_i^0, \text{ for } i \in \text{bottom nodes}, \end{aligned} \tag{S10}$$

where z_i^0 denotes the initial z position of the i-th nodes. In all simulations, the width of the sample w_0 in the x-direction is set to two times of its height h_0 as $w_0 = 2h_0$. To limit boundary effects on the left and right surfaces and enforce a pure shear loading condition, we further fix their x-displacement via

$$\begin{aligned} x_i &= x_i^0, \text{ for } i \in \text{left nodes}, \\ x_i &= x_i^0, \text{ for } i \in \text{right nodes}, \end{aligned} \tag{S11}$$

where x_i^0 denotes the initial x position of the i-th nodes. Eqs. (S9-S11) form a boundary value problem that can be solved numerically.

S2.2 Quasi-static solver

As discussed in the previous subsection, the coordinates of every node (x_i, y_i, z_i) fully describe the state of the system. Therefore, all system variables can be written in vector form:

$$\mathbf{X} = [x_1, y_1, z_1, x_2, y_2, z_2, ..., x_n, y_n, z_n]^T. \tag{S12}$$

The vector $\mathbf{X}$ is a $3n$ by 1 vector containing all the information we need to describe the deformation of the lattice. To obtain $\mathbf{X}$, we solve the nonlinear system of equations illustrated by Eqs. (S9-S11), which can be written generally as,

$$\mathbf{F}(\mathbf{X}) = \mathbf{0}. \tag{S13}$$

Note that the equation above presents the same governing equations as Eq. (S9).

Newton's method is implemented to solve the governing equation (Eq.(S13)). The generalized Newton's method is to find a root of a functional $\mathbf{F}$ defined in a Banach space. In this case, the formulation is

$$\mathbf{X}_{l+1} = \mathbf{X}_l - \Big[\mathbf{J}(\mathbf{X}_l)\Big]^{-1}\mathbf{F}(\mathbf{X}_l), \tag{S14}$$

where $\mathbf{J}(\mathbf{X}_l)$ is the Jacobian matrix of the function $\mathbf{F}$ at $\mathbf{X}_l$, and l is the iteration number. Instead of computing the inverse of this matrix, one can save time by solving the following system of linear equations:

$$\mathbf{J}(\mathbf{X}_l)\,(\mathbf{X}_{l+1} - \mathbf{X}_l) = -\mathbf{F}(\mathbf{X}_l). \tag{S15}$$

Starting with some initial guess $\mathbf{X}_0$, the next approximate solution $\mathbf{X}_l$ can be obtained iteratively. The method ends when $\|\mathbf{X}_{l+1} - \mathbf{X}_l\| < \delta$, where δ is a defined accuracy requirement.

To simulate the quasi-static response of the system, the loading process is divided into P steps, which gradually stretch the lattice. At each step, the state of the system $X^{(p)}$ is obtained by solving Eq. (S13), where $p = 1, .., P$. Furthermore, we always use the solution of the current step as the initial guess for the next step to accelerate convergence of the Newton's method.

S2.3 Dynamic solver

To simulate the dynamic response of the lattice, we add inertia and dissipation terms to the previous governing equation Eqs. (S9), yielding:

$$\begin{aligned} M\ddot{x}_i &= \frac{\partial U_{\text{total}}}{\partial x_i} + \beta M\dot{x}_i, \\ M\ddot{y}_i &= \frac{\partial U_{\text{total}}}{\partial y_i} + \beta M\dot{y}_i, \\ M\ddot{z}_i &= \frac{\partial U_{\text{total}}}{\partial z_i} + \beta M\dot{z}_i, \end{aligned} \tag{S16}$$

where M is the assigned pseudo-mass at each node and β is the damping coefficient. Similarly, governing equations Eqs. (S16) can be written generally in vector form as

$$M\ddot{\mathbf{X}} = \mathbf{F}(\mathbf{X}) + \beta M\dot{\mathbf{X}}. \tag{S17}$$

Note that $\mathbf{F}(\mathbf{X})$ in the above equation is identical as the one in quasi-static problems (Eq. (S13)). Eq. (S17) is solved via the Runge–Kutta method using the `ode45` function in MATLAB.

As the initial condition, the lattice is loaded near fracture of the first bridging chain of an artificial crack, which is the result of the quasi-static simulation. The bridging chain is artificially broken (removed) at the crack tip, perturbing the system out of equilibrium at time $t = 0$. The nodes accelerate, vibrate, and dissipate energy until a new equilibrium state is achieved. We simulate the system from time $t = 0$ to $t = t_0$, where t_0 is selected to be large enough such that the kinetic energy of the whole system approaches zero. The solution of Eq. (S17) yields time evolution of the state variables, i.e., $\mathbf{X}(t)$, where $t \in [0, t_0]$.

S2.3.1 Distribution of dissipated energy

The energy dissipated $\mathcal{D}$ at node i can be calculated by integrating the work done by the damping force over time,

$$\mathcal{D}_i = \int_0^{t_0} \beta M \left(\dot{x}_i^2 + \dot{y}_i^2 + \dot{z}_i^2\right) dt. \tag{S18}$$

The spatial distribution of $\mathcal{D}_i$ around the crack tip demonstrates the dispersion of energy within the sample following the fracture of one chain. Theoretically, the value of dissipation friction β quantitatively affects the distribution of $\mathcal{D}_i$. For example, when $\beta \to 0$ the released energy will be emitted in the form of dynamic waves propagating circumferentially from the crack tip to the periphery of the sample. However, as demonstrated in Fig. S2, the value of β does not qualitatively alter the spatial distribution of $\mathcal{D}_i$ given that β is large enough. In this case, the whole system is overdamped, and the exact value of β does not make a difference. For the present simulations, we pick $\beta = 1$.

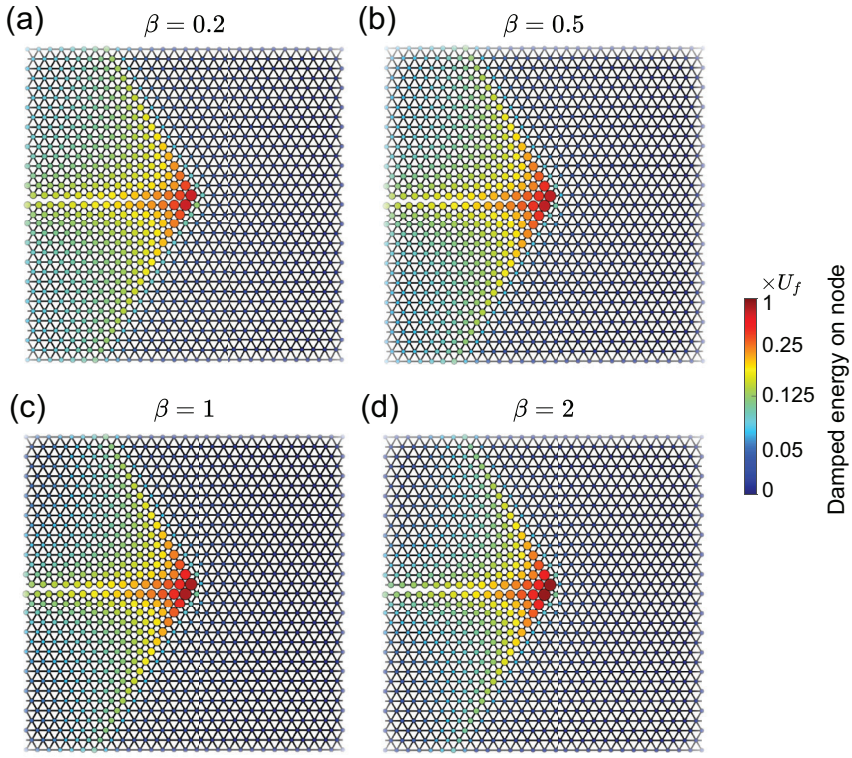

Figure S2: Dynamic simulation results for dissipation coefficient (a) $\beta = 0.2$, (b) $\beta = 0.5$, (c) $\beta = 1$, and (d) $\beta = 2$. Energy dissipated at each node $\mathcal{D}_i$ is illustrated by its color and size. There is no qualitative difference between dissipation distribution for different β.

S2.3.2 Size of dissipation zone

In this section, we aim to elucidate the scale of the dissipation zone within polymer-like networks using a network comprised of PEG chains with a damping coefficient $\beta = 1$. Fig. S3(a) exhibits the distribution of dissipated energy for visualization of the extent of the dissipation zone. This illustration shares the same network structure presented in Fig. 4(d) of the main manuscript and Fig. S2(c) yet offers a more detailed view. Specifically, the left panel of Fig. S3(a) portrays the distribution over 120 layers, whereas the right panel provides a close-up inspection of 50 layers. In contrast, Fig. 4(d) in the main manuscript only includes 16 layers. As is evident from Fig. S3(a), the dissipation zone in polymer-like networks spans multiple layers, extending far from the crack tip.

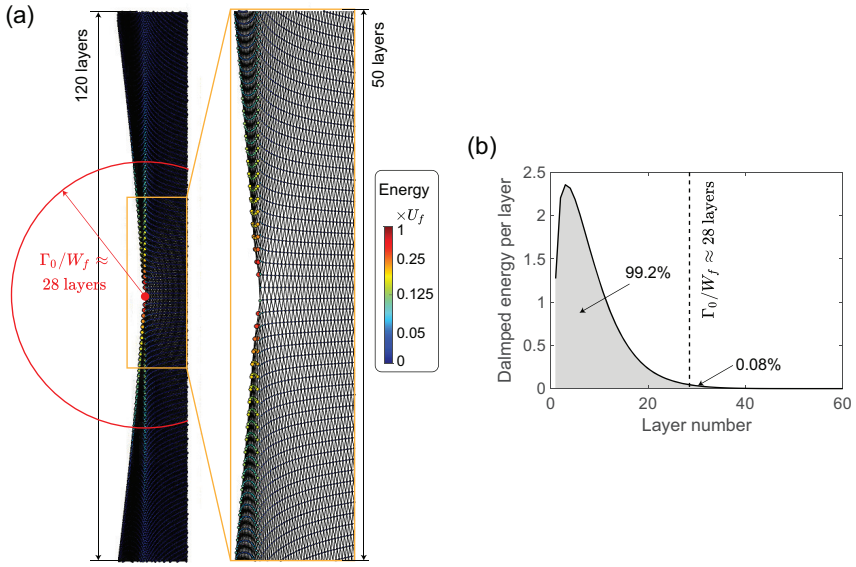

Figure S3: Analysis of the dissipation zone in the polymer-like network with PEG chains. (a) The distribution of dissipated energy is visualized across a broader range of layers than shown in the manuscript. The circle represents a distance of $\Gamma_0/W_f = 28$ layers from the crack tip, providing an estimate of the dissipation zone size. (b) The dissipated energy plotted as a function of the number of layers from the crack tip. The graph indicates that approximately 99.2% of the energy is dissipated within the span of $\Gamma_0/W_f = 28$ layers.

Given these observations, it is pertinent to question if the dissipation zone size can be pre-

dicted. In the realm of nonlinear fracture mechanics, the ratio of intrinsic fracture energy, Γ_0 [J/m^2], and the material's work to failure, W_f [J/m^3], gives the flaw sensitively length L_s, which is a relevant length scale (*14*). In highly stretchable network structures, the work to failure, W_f, is given by $W_f = MU_{\text{chain}}/L_0$, where U_{chain} represents the work to rupture a single chain, M denotes the area density, and L_0 is the unperturbed contour length of the chain. Notably, the Lake-Thomas model postulates that $\Gamma_{\text{LT}} = MU_{\text{chain}}$, leading to the relationship $W_f = \Gamma_{\text{LT}}/L_0$. Consequently, the flaw sensitivity length scale, L_s, can be expressed as

$$L_s = \Gamma_0/W_f = (\Gamma_0/\Gamma_{\text{LT}})\, L_0. \tag{S19}$$

In the context of the PEG chains analyzed here, this translates to a length scale of $\Gamma_0/W_f \approx 28L_0$. A representation of this span – equivalent to $28L_0$ – is depicted in Fig.S3(b), which closely matches the observed size of the dissipation zone. To delve deeper, the dissipated energy was quantified against the layer number from the crack tip, as shown in Fig.S3(a). Results indicate that 99.2% of the dissipated energy comes from within the first 28 layers (i.e., within $28L_0$), suggesting that the flaw sensitivity length Γ_0/W_f can offer an estimate of the dissipation zone scale. The implications of this discovery are profound, for the L_s parameter discussed throughout could offer a tangible measure of the dissipation zone size. Furthermore, in scenarios where $\Gamma_0 = \Gamma_{\text{LT}}$, it can be deduced that $L_s = L_0$, implying that all dissipated energy is attributed to the fracturing chain. In this case, all the energy is dissipated by the breaking chain, which is a direct reflection of the Lake-Thomas model.

S2.4 Convergence

The value of intrinsic fracture energy measured through the pure-shear test is not affected by the number of vertical layers, given that the sample is thick enough in y-direction. Note that in this work, x-direction aligns with the horizontal width direction of the sample, y-direction aligns with the vertical loading direction, and z-direction denotes the out-of-plane thickness

direction. In this section, we investigate the number of vertical layers required for the measured network intrinsic fracture energy Γ_0 to converge. Here, we use a 2D triangular lattice as an example; these results are transferable to other 2D and 3D network topologies. In Fig. S4, we report the value of Γ_0 as a function of vertical layer number for one network of linear chains and two networks of polymer-like chains with different ratios of $K_{\mathrm{E}}/K_{\mathrm{S}}$. For the linear network (Fig. S4a), Γ_0 converges within 4 vertical layers and remains unchanged with increasing size. This is consistent with the physical picture of the Lake-Thomas model, where all the energy is released and dissipated on the layer on the crack tip. However, for the polymer-like networks with $K_{\mathrm{E}}/K_{\mathrm{S}}$ =1.8 $\times$ 10^3 (Fig. S4b, this value is one tenth that of PEG chains), the value of Γ_0 does not converge until about 100 vertical layers. As the polymer-like chains become more nonlinear – as in the case of PEG chains with $K_{\mathrm{E}}/K_{\mathrm{S}}$ =1.8 $\times$ 10^4 – the sample requires more than 2000 vertical layers for the intrinsic fracture energy value to converge ((Fig. S4c). These simulation results suggest that as the nonlinearity of chain constitutive behavior increases, the number of vertical layers needed to achieve a converged value of intrinsic fracture energy increases. This implies that the energy releasing and dissipation processes for polymer-like chains are delocalized compared to the linear ones. In all simulation results presented in the manuscript, we use samples with 4000 vertical layers to ensure convergence.

S2.5 Coarse-graining the network

As discussed in the previous section, we need to simulate networks with on the order of thousands of layers to ensure convergence. As a case study, a 2D triangular network with 4000 layers consists of $\sim$40 million nodes. Since each node has two degrees of freedom (DOFs) in 2D space, the network contains $\sim$80 million degrees of freedom. The size of the resulting Jacobian matrix $\mathbf{J}$ in Eq. (S14) is $\sim$80 million $\times$ 80 million. Currently, common desktops struggle to handle systems with 1 million DOFs. Since the complexity of solving linear systems is at

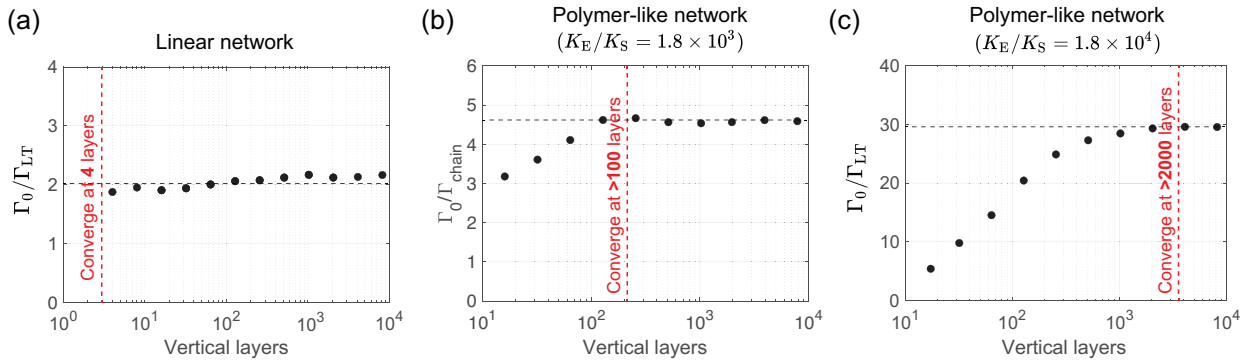

Figure S4: Convergence study for (a) linear network, (b) polymer-like network with $K_E/K_S = 1.8 \times 10^3$ (one tenth of the PEG chain), and (c) polymer-like network with $K_E/K_S = 1.8 \times 10^4$ (PEG chain). Linear network converged within 4 layers, polymer-like chain with $K_E/K_S = 1.8 \times 10^3$ converged at around 100 layers, and polymer-like chain with $K_E/K_S = 1.8 \times 10^4$ converged at around 2000 layers.

least $O(n^2)$, our system with 80 million DOFs requires at least 6400 times more computational resources than a system with 1 million DOFs. Memory overflow is also a challenge for this kind of problem; moreover, our simulations must repeatedly solve such linear systems $\sim$1000 times. Therefore, it is impractical to directly simulate a network of this size.

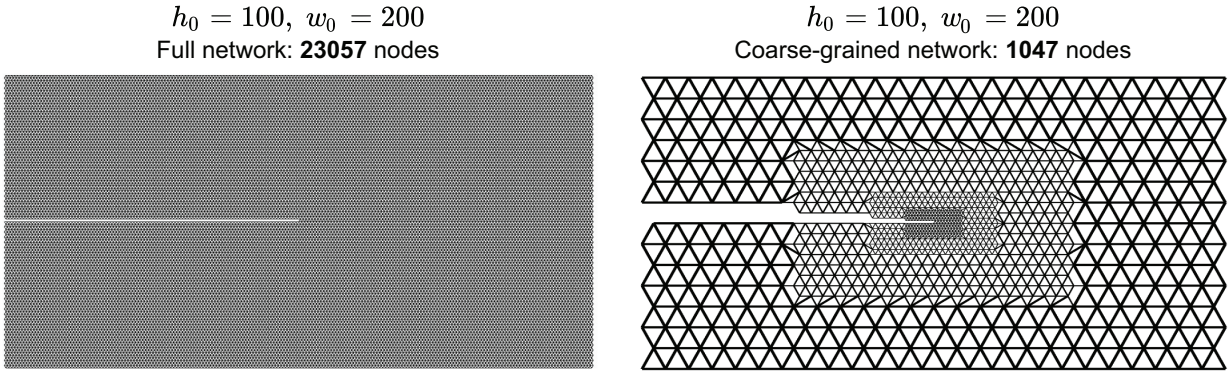

Figure S5: Hierarchically coarse-grained network compared to its corresponding full network. The thicknesses of the edges are proportional to their relative stiffnesses. The coarse-grained method decreases the total node number from 23057 to 1047.

To accelerate the simulation of large size networks, we developed a hierarchical coarse-grained method to reconstruct the network with significantly fewer DOFs. Near fracture of the bridging chain, the network is most inhomogeneous near the crack but becomes more homo-

geneous with increasing distance from the crack tip. Since chains far from the crack tip do not drastically vary within their local neighborhood, a coarser lattice can equivalently represent the effect of these neighborhoods on the continuum level. As an example, a 2D triangular network with $h_0 = 100$ layers and $w_0 = 200$ layers can be reconstructed with a few levels of coarse-grained lattices as shown in Fig. S5. In the coarse-grained network, the relative stiffness of chains is set to be proportional to their length (represented by line thicknesses in Fig. S5). This ensures that the coarse-grained network has the same bulk mechanical performance as the full network. A full network consisting of 23,057 nodes can be hierarchically coarse-grained to possess only 1047 nodes. The coarse-grained model still accurately predicts the critical stretch at which the first chain breaks. Although the coarse-grained model cannot accurately predict the full fracture process, it is sufficient to yield an accurate assessment of h_c, as defined for the pure-shear test.

To substantiate our claims, we carry out a pure shear test using numerical simulations on two types of networks with $h_0 = 100$ layers and $w_0 = 200$ layers: a full network and a hierarchical coarse-grained network. When subjected to a notched test, the full network generates $h_c = 495.6r_0$ (note that r_0 denotes the rest length of each edge), while the coarse-grained network exhibits $h_c = 495.1r_0$, reflecting a marginal error of just 0.1%. Further, when evaluating the fracture energy, the full network demonstrates a ratio of $\Gamma_0/\Gamma_{\text{LT}} = 18.31$, whereas the coarse-grained network yields a ratio of $\Gamma_0/\Gamma_{\text{LT}} = 17.91$, implying a minor error of 2.1%. These results compellingly validate that the coarse-grained network can be reliably used to predict the intrinsic fracture energy of the full network.

In Fig. S6, we present the actual coarse-grained triangular network we used for simulations. The network has a size of $h_0 = 4000$ layers by $w_0 = 8000$ layers, with a total of 44,847 nodes and 89,694 DOFs. Note that the full network with the same size would require 40 million nodes, so our hierarchical coarse-grained method decreases the required number of DOFs by 99.9%.

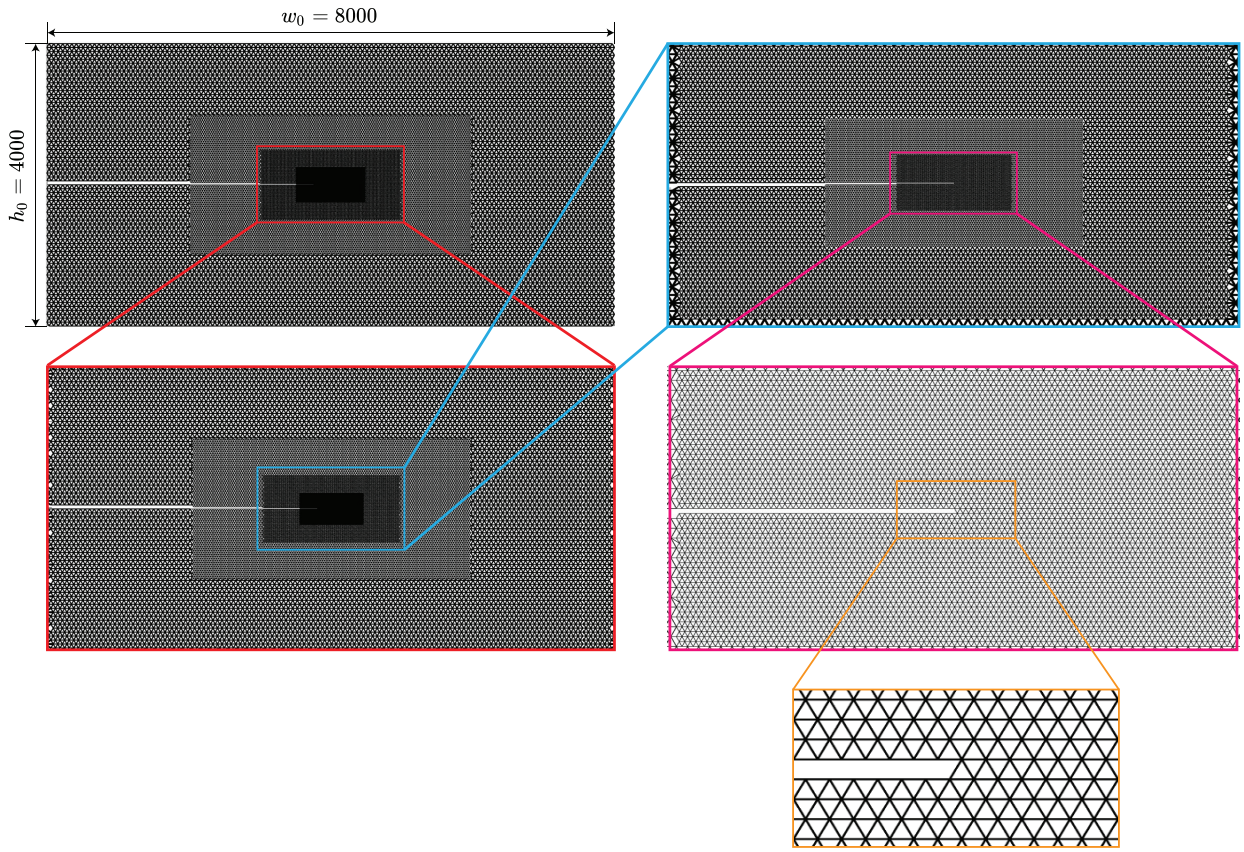

Figure S6: The coarse-grained 2D triangular network used in our simulations. The network has a size of $h_0 = 4000$ layers by $w_0 = 8000$ layers, with 44,847 total nodes.

The coarse-grained network provides a moderate matrix size that can be easily computed by common computers. Each iteration of Newton's method – including the assembly of Jacobian matrix and solving Eq. (S14) – costs a few seconds. The whole simulation of the fracture of a $h_0 = 4000$ layer network typically takes $15-20$ minutes to complete on a standard desktop with Intel Core i9- 12900K.

S3 Fabrication and Testing

S3.1 Fabrication

Specimens were fabricated by laser cutting Wear-Resistant Easy-to-Machine Acetal Films (12" x 12" x 0.003") (McMaster-Carr part number: 5742T11) using an EpilogLaser Zing 24 60W laser machine. The pattern was designed using CorelDraw with 12 layers of triangular repeating units and 27 strands per layer (Fig. S7). Each strand has a "zigzag" structure that can unfold to provide an initial soft bending, followed by a stiff stretching due to the deformation of the material (*15*). This large discrepancy between stiffness mimics the force-extension behavior of polymer chains. The distance between the laser head and the acetal film was calibrated as instructed in the machine's operating manual to ensure sharp focus. The parameters were chosen to be 10% of the laser power, 10% of the frequency, and 100% of the speed. Four identical samples in total were cut to perform the measurement of energy release rate. For each sample, four 1/16" acrylic sheets were cut and glued onto the front and the back of the uncut portion to act as rigid boundary (manuscript figure 5b), which was clamped onto the mechanical testing machine.

S3.2 Testing

Mechanical tests were performed on ZwickiLine tensile testing machine (Zwick Roell). To measure the fracture energy Γ_0, we conducted uniaxial extension on an unnotched sample at a loading rate of 100 mm/min (Fig. S7), as shown by the solid black line in Fig. 5c of the manuscript. Using the obtained force-stretch curve, we inversely identified the effective force-stretch curve for each strand (the curve shown in Fig. 5c of the manuscript) such that the simulation results match with the experimental measurements. For the other three samples, we introduced a notch at the same position on each sample to yield three identical notched samples. Uniaxial tensile tests were performed on the three notched samples at a loading rate of 100 mm/min. Since the

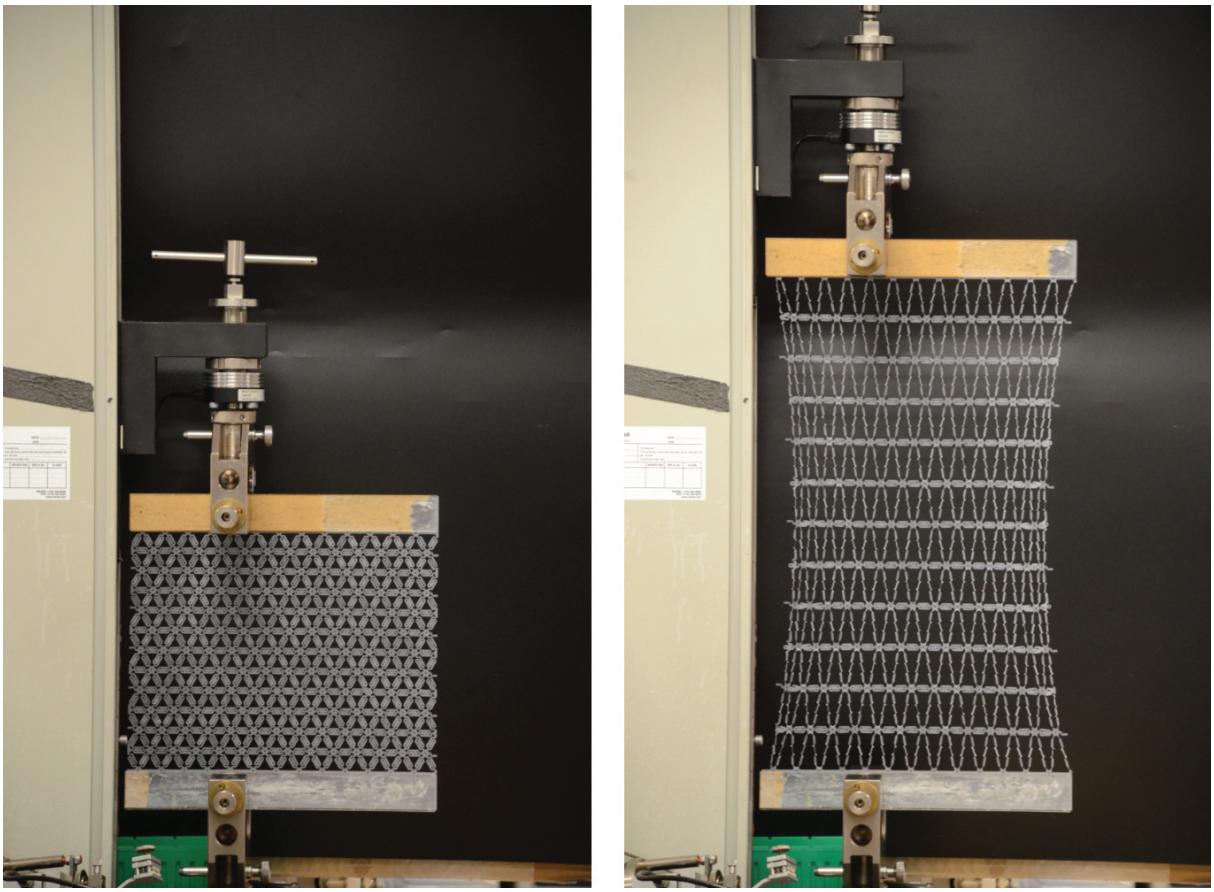

Figure S7: The laser cut network glued with rigid acrylic boundary is clamped onto the Zwick Roell tensile tester (left) and stretched (right) to record the force-stretch curve

rupture of strands is uncontrolled when a notched sample is loaded to the fracture event, we pre-set a critical stretch of 2 and consider the bridging strands to have "ruptured" when the whole network reaches the critical stretch. The energy release rate at the stretch of 2 is considered to be the intrinsic fracture energy Γ_0 of the network. By integrating the force-extension curve of unnotched sample to the stretch of 2 times to the initial height of the network $h_0 = 207.8$ mm, we obtained the intrinsic fracture energy for the network to be $\Gamma_0 = 321.2$ mJ.

To compare with the Lake-Thomas model, the stretch of the bridging strand at the crack tip is measured using calipers when the notched sample reached the critical stretch of 2. Three bridging strands for three notched samples were measured to be 37.85 mm, 38.25 mm, and

37.33 mm when the sample stretch reached 2. Since the undeformed strands each have a length of 20.00 mm, the average critical stretch for the bridging strands was calculated to be 1.89. By integrating the force-stretch curve of a single strand up to a stretch of 1.89 and multiplying this integration by $M = 27$ (the number of strands in a layer), the Lake-Thomas Model estimated the fracture energy $\Gamma_{\text{LT}} = MU_{\text{chain}} \approx 57.7$ mJ. Hence, the ratio $\Gamma_0/\Gamma_{\text{LT}} = 5.57$ is significantly larger than unity but consistent with our model's expectation that a significant amount of energy would be released from far from the crack tip.

References

1. F Oesterhelt, M Rief, and HE Gaub. Single molecule force spectroscopy by afm indicates helical structure of poly (ethylene-glycol) in water. *New Journal of Physics*, 1(1):6, 1999.

2. Hubert M James and Eugene Guth. Theory of the elastic properties of rubber. *The Journal of Chemical Physics*, 11(10):455–481, 1943.

3. Michael Rubinstein, Ralph H Colby, et al. *Polymer physics*, volume 23. Oxford university press New York, 2003.

4. Shu Wang, Sergey Panyukov, Stephen L Craig, and Michael Rubinstein. Contribution of unbroken strands to the fracture of polymer networks. *Macromolecules*, 2023.

5. Shu Wang, Haley K Beech, Brandon H Bowser, Tatiana B Kouznetsova, Bradley D Olsen, Michael Rubinstein, and Stephen L Craig. Mechanism dictates mechanics: a molecular substituent effect in the macroscopic fracture of a covalent polymer network. *Journal of the American Chemical Society*, 143(10):3714–3718, 2021.

6. Christopher W Barney, Ziyu Ye, Ipek Sacligil, Kelly R McLeod, Han Zhang, Gregory N Tew, Robert A Riggleman, and Alfred J Crosby. Fracture of model end-linked networks. *Proceedings of the National Academy of Sciences*, 119(7):e2112389119, 2022.

7. Bobin Lee, Zhenbin Niu, Junpeng Wang, Carla Slebodnick, and Stephen L Craig. Relative mechanical strengths of weak bonds in sonochemical polymer mechanochemistry. *Journal of the American Chemical Society*, 137(33):10826–10832, 2015.

8. Shaoting Lin, Jiahua Ni, Dongchang Zheng, and Xuanhe Zhao. Fracture and fatigue of ideal polymer networks. *Extreme Mechanics Letters*, 48:101399, 2021.

9. Yuki Akagi, Jian Ping Gong, Ung-il Chung, and Takamasa Sakai. Transition between phantom and affine network model observed in polymer gels with controlled network structure. *Macromolecules*, 46(3):1035–1040, 2013.

10. GJ Lake and AG Thomas. The strength of highly elastic materials. *Proceedings of the Royal Society of London. Series A. Mathematical and Physical Sciences*, 300(1460):108–119, 1967.

11. Hanako Asai, Kenta Fujii, Takeshi Ueki, Takamasa Sakai, Ung-il Chung, Masayoshi Watanabe, Young-Soo Han, Tae-Hwan Kim, and Mitsuhiro Shibayama. Structural analysis of high performance ion-gel comprising tetra-peg network. *Macromolecules*, 45(9):3902–3909, 2012.

12. Yuki Akagi, Hayato Sakurai, Jian Ping Gong, Ung-il Chung, and Takamasa Sakai. Fracture energy of polymer gels with controlled network structures. *The Journal of chemical physics*, 139(14):144905, 2013.

13. Shaoting Lin and Xuanhe Zhao. Fracture of polymer networks with diverse topological defects. *Physical Review E*, 102(5):052503, 2020.

14. Chao Chen, Zhengjin Wang, and Zhigang Suo. Flaw sensitivity of highly stretchable materials. *Extreme Mechanics Letters*, 10:50–57, 2017.

15. Kyung-In Jang, Ha Uk Chung, Sheng Xu, Chi Hwan Lee, Haiwen Luan, Jaewoong Jeong, Huanyu Cheng, Gwang-Tae Kim, Sang Youn Han, Jung Woo Lee, et al. Soft network composite materials with deterministic and bio-inspired designs. *Nature communications*, 6(1):6566, 2015.